A molecular orbital investigation of the diamagnetism and stability of triangular 50-electron M_3L_n clusters

Maria Teresa Garland,[a] Karine Costuas,[b] Samia Kahlal[b] and Jean-Yves Saillard*[b]

[a] *Laboratorio de Cristalografía, Universidad de Chile, Casilla 487-3, Santiago, Chile*
[b] *Laboratoire de Chimie du Solide et Inorganique Moléculaire (UMR CNRS 6511), Université de Rennes 1, 35042 Rennes cedex, France.*

Received (in Strasbourg, France) 14th January 1999, Accepted 16th March 1999

EHT and DFT calculations have been carried out on a series of triangular 50-electron M_3L_n clusters and of other electron-rich related species in order to understand why they are both diamagnetic and Jahn–Teller stable, although they exhibit weak M—M bonding. The six MOs associated with the M_3 skeleton are combinations of σ and π_σ frontier orbitals on the metal centers. In all these compounds the large calculated HOMO–LUMO gap is the consequence of two major factors: (*i*) the σ hybrid-type of the hybrid-type e′* LUMO, which maintains it at a high energy despite its weak antibonding character and (*ii*) the π_σ d-type character of the occupied out-of-phase a'_2* level, which maintains it at low energy. On the other hand, at the considered internuclear separations the a'_1 in-phase combination of the σ metal hybrids always has enough bonding character to be low-lying. The particularly low energy position of the a'_2* level, which contains the two extra electrons, is the result of the particular orientation of the ligands around the metal centers, which controls the orientation, the hybridization and the energy of the π_σ frontier orbitals. The presence of π-donor in-plane bridging ligands strongly favors the stability of these electron-rich clusters, while terminal-only ligands or π-acceptor bridging ligands do not. The M—M bonding character is mainly contained in the a'_1 skeletal MO. Cluster core isomerism is discussed with respect to the opening of one M—M edge of the triangle.

Organometallic M_3L_n clusters presenting a regular triangular metallic framework possess generally a total metal valence electron (MVE) count of 48, in accordance with the 18-electron rule and the presence of M—M single bonds. Examples of MVE counts lower than 48 are known. Their stability can be generally rationalized through the existence of localized or delocalized multiple bonding[1] or by the presence of 16-electron metal centers lying in a planar coordination environment (see below). The formal addition of 2 electrons to a 48-MVE system is expected to result in the breaking of one M—M bond, leading to an open M_3 triangle in which the metal centers still obey the 18-electron rule. There are, however, examples of regular and more-or-less regular 50-MVE triangular clusters in which the M—M bonds are generally longer that what one would expect for localized 2-electron 2-center bonds.[2–8] These compounds are listed in Table 1*a*, together with their reported M—M bond distances. Related clusters of higher nuclearity that can be described as containing a 50-MVE triangle are listed in Table 1*b*.[9–12] In all these clusters, the metal triangle is bridged by μ_2 or μ_3 ligands, which may be interpreted as indicative of some intrinsic weakness of the metallic framework. However, this seems contradictory with the stability and diamagnetic behavior of these species, which suggest the existence of a significant (if not large) HOMO–LUMO gap. This has been confirmed by theoretical extended Hückel theory (EHT) investigations on some of these complexes.[3,4,11*b*,19] Using the results of these previous studies as well as simple symmetry arguments, one can simply describe the metal electronic structure of these electron-rich clusters as follows.

Starting from a regular 48-MVE M_3L_n species of ideal D_{3h} symmetry, group theory considerations lead to a description of the 3 localized M—M bonds as formed by 3 occupied bonding MOs of a_1 and e′ symmetry and 3 unoccupied antibonding MOs of a'_2 and e′ symmetry, as sketched in Fig. 1(*a*). In a 50-MVE species, there are 2 extra electrons in the antibonding system. The occupation of the antibonding e′* level would induce either a paramagnetic behavior or more likely a first-order Jahn–Teller distortion, which would lead to the breaking of one M—M bond. It turns out that in all the calculated 50-MVE species, the occupied M—M antibonding orbital is found to be the non-degenerate a'_2* level.[3,4] However, this is not a sufficient condition to stabilize a diamagnetic triangular system. Indeed, a small HOMO(a'_2*)–LUMO(e′*) gap would induce a second-order Jahn–Teller distortion or lead to some paramagnetism. In the previously calculated models, the a'_2* level was always found to lie at a surprisingly low energy considering its out-of-phase character, and the associated HOMO–LUMO gap is computed to be large,[3,4] as schematized in Fig. 1(*b*). Therefore, while the stability and diamagnetism of the triangular 50-MVE clusters seems to be understood, important questions remain: why, in all these 50-MVE species, is the occupied M—M a'_2* anti-

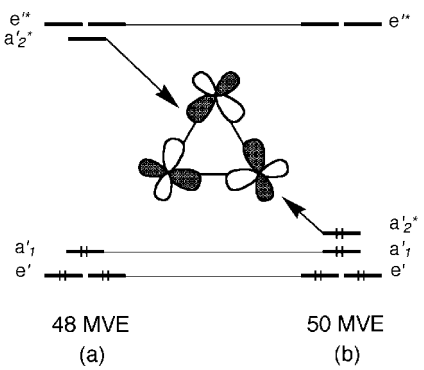

Fig. 1 The molecular orbitals associated with M—M bonding in a diamagnetic M_3L_n regular triangular cluster: (*a*) 48-MVE species, (*b*) 50-MVE species.

Table 1 Structurally characterized 50-MVE M_3L_n triangular clusters and related compounds: M—M bond distances and some EHT-computed data

Compound	M—M distance/Å	M—M overlap population	HOMO–LUMO gap/eV	Reference
(*a*) 50-MVE M_3 systems				
(**1**)[a] $[Mo_3(\mu_3\text{-Bi})(\mu_3\text{-OMe})_3(CO)_9Mo(CO)_3]^{2+}$	3.077, 3.087, 3.082	0.080, 0.073, 0.079	1.58	2
(**2**)[b] $Mo_3[\mu_3\text{-AsMo}(CO)_5](\mu_3\text{-OMe})_3(CO)_9Mo(CO)_3]^{2+}$	3.037, 3.022, 3.048	0.063, 0.062, 0.061	0.99	3
(**3**) $Ru_3(\mu_3\text{-}\eta^2\text{-PPhpy})(\mu\text{-PPh}_2)_3(CO)_9$	3.112, 3.085, 3.112	0.054, 0.058, 0.035	1.55	4
(**4**) $Ru_3(\mu\text{-Cl})(\mu\text{-PPh}_2)_3(CO)_7$	2.929, 3.222, 3.129	0.060, 0.049, 0.070	1.87	5
(**5**) $Ru_3(\mu_3\text{-H})(\mu\text{-PPh}_2)_3[\mu\text{-P(Ph)C}_6H_4](CO)_6$	3.034, 3.207, 3.146	−0.006, 0.000, 0.005	2.21	6
(**6**) $Os_3(\mu_2\text{-}\eta^2\text{-CCPr}^i)_2(\mu\text{-PPh}_2)_2(CO)_7$	2.972, 3.246, 3.101	0.111, 0.078, 0.110	2.30	7
(**7**) $Rh_3(\mu\text{-PPh}_2)_3(CO)_7$	3.123, 3.222, 3.083	0.031, 0.010, 0.013	1.54	8
(**8**) $Rh_3(\mu\text{-PPh}_2)_3(CO)_6(PPh_2H)$	3.117, 3.245, 3.130	0.019, 0.000, 0.019	1.58	8
(*b*) Metal-bridged 50-MVE M_3 systems				
(**9**) $Ru_3(\mu_2\text{-}\sigma_1\text{-}\eta^2\text{-CCBu}^t)(\mu\text{-PPh}_2)[\mu\text{-Ru}(CO)_4](CO)_9$	3.157, 3.197, 3.025	0.067, 0.049, 0.123[c]	1.28	9
(**10**) $Ru_3(\mu\text{-PPh}_2)_2[Fe(CO)_4](CO)_9$	3.148, 3.171, 3.098	0.047, 0.053, 0.107[c]	1.36	10
(**11**) $Ru_3(\mu\text{-PPh}_2)_2[Ru(CO)_4](CO)_9$	3.178, 3.178, 3.051	0.051, 0.051, 0.116[c]	1.26	11
(**12**) $Ru_3(\mu\text{-PPr}^i_2)_2[Ru(CO)_4](CO)_9$	3.199, 3.160, 3.076	0.050, 0.057, 0.116[c]	1.23	11
(**13**) $Ru_3[\mu\text{-PNPr}^i_2]_2[Ru(CO)_4](CO)_9$	3.106, 3.106, 3.159	0.064, 0.064, 0.099[c]	1.20	11
(**14**) $Ru_3[\mu\text{-P(OEt)}_2]_2[Ru(CO)_4](CO)_9$	3.232, 3.218, 3.032	0.042, 0.045, 0.130[c]	1.20	11
(*c*) Related 44-MVE M_3 systems				
(**15**) $Pd_3(\mu\text{-PBu}^t_2)_3(Cl)(CO)_2$	2.949, 2.949, 3.000	0.065, 0.065, 0.052	1.56	12
(**16**) $[Pd_3(\mu\text{-PPh}_2)_2(\mu\text{-Cl})(PPh_3)_3]^+$	2.933, 2.936, 2.906	0.067, 0.063, 0.053	1.27	13
(**17**)[d] $[Pd_2Pt(\mu\text{-PPh}_2)_2(\mu\text{-Cl})(PPh_3)_3]^+$	2.878, 2.886, 2.908	0.053, 0.092, 0.086	1.61	13
(**18**) $[Pd_3(\mu\text{-PPh}_2)_2(\mu\text{-Cl})(PEt_3)_3]^+$	2.935, 2.928, 2.894	0.066, 0.070, 0.062	1.30	14
(**19**) $Pd_3(\mu\text{-SO}_2)_2(CNBu^t)_5$	2.734, 2.734, 2.760			15
(**20**) $Pt_3(\mu\text{-PPh}_2)_3(PPh_3)_2(Ph)$	2.956, 2.956, 3.074	0.085, 0.085, 0.081	1.80	16
(**21**) $[Pt_3(\mu\text{-SO}_2)_2(\mu\text{-Br})(PCy_3)_3]^-$	2.887, 2.887, 2.883	0.133, 0.133, 0.104	2.59	17
(*d*) Related metal-bridged 44-MVE M_3 system				
(**22**) $\{Pt_3[\mu\text{-Fe}(CO)_4]_3(CO)_3\}^{2-}$	2.751, 2.755, 2.743	0.197,[c] 0.197,[c] 0.193[c]	1.39	18[e]

a One Mo atom is not directly bonded to the Mo_3 triangle. *b* Two Mo atoms are not directly bonded to the Mo_3 triangle. *c* Metal-bridged M—M bond. *d* Non-stoichiometric compound ($Pd_{2.19}Pt_{0.81}$). The approximate stoichiometry Pd_2Pt was considered in the calculations.

bonding orbital lying at a much lower energy than the other M—M antibonding level e′* [Fig. 1(*b*)]? Why is the a'_2* level high-lying in the case of the regular 48-MVE compounds [Fig. 1(*a*)]? In order to provide a better insight into the electronic and structural factors that control differently the energies of the a'_2* and e′* levels, we have undertaken a theoretical investigation of the electronic structure of these triangular clusters. Calculations were carried out using both EHT and density functional theory (DFT) methods. Details of the calculations are given below.

Computational details

EHT calculations[20] were carried out using the CACAO package.[21] The weighted H_{ij} formula was considered.[22] The atomic parameters used for H to Br are the standard ones.[20] For the other elements, the valence ns and np exponents (ξ) and the valence shell ionization potentials (H_{ii} in eV) are given below. 6s(**Bi**): 2.653, −15.75; 6p(**Bi**): 2.092, −10.52; 5s(Ru): 2.078, −8.6; 5p(Ru): 2.043, −5.1; 5s(Rh): 2.135, −8.09; 5p(Rh): 2.100, −4.57; 5s(**Pd**): 2.190, −7.32; 5p(**Pd**): 2.152, −3.75; 6s(**Pt**): 2.554, −9.08; 6p(Os): 2.300, −8.17; 6s(Os): 2.300, −4.81; 6p(**Pt**): 2.554, −5.47. The transition metal ($n-1$)d valence orbitals were described by a linear combination of two Slater-type orbitals of exponents ξ_1 and ξ_2 with the weighting coefficients C_1 and C_2. The ($n-1$)d parameters are listed below in the order ξ_1, ξ_2, C_1, C_2, H_{ii}. 4d(Ru): 5.378, 2.303, 0.534, 0.637, −12.20; 4d(Rh): 5.680, 2.450, 0.544, 0.653, −12.50; 4d(**Pd**): 5.983, 2.613, 0.554, 0.670, −12.02; 5d(Os): 5.000, 2.100, 0.666, 0.541, −11.84; 5d(**Pt**): 6.013, 2.696, 0.633, 0.551, −12.59. In the calculated models the following bond distances (Å) were assumed: Ru—CO(terminal) = 1.88; Ru—CO(bridge) = 2.15; Ru—P = 2.36; Ru—Cl = 2.45; C—O = 1.14; P—H = 1.42. All the Walsh diagrams were calculated assuming variation of the Ru—Ru separation, all the other bond distances being kept constant. Calculations on the compounds of Table 1 were run on the X-ray molecular structures obtained from the Cambridge Data Base system.[23] When unavailable, hydrogen atoms were placed at calculated positions. Due to their large number of atoms, compounds **16**, **17** and **20** were simplified by replacing some alkyl or phenyl groups by hydrogen atoms.

DFT calculations[24] were carried out using the Amsterdam Density Functional (ADF) program.[25] Electron correlation was treated within the local density approximation in the Vosko–Nusair parametrization (LDA).[26] The numerical integration procedure applied for the calculations was developed by te Velde and Baerends.[24d] A triple-ζ Slater-type orbital (STO) basis set was used for Ru 4d and 5s augmented with a single-ζ 5p polarization function. A double-ζ STO basis set was employed for H 1s, C and O 2s and 2p, P and Cl 3s and 3p, extended with a single-ζ polarization function 2p for H and 3d for C, O, P and Cl. A frozen-core approximation was used to treat the core electrons of C, O, P, Cl and Ru.[24a]

Results and discussion

The 50-MVE $[Ru_3(\mu\text{-PH}_2)_3(CO)_9]^+$ and $[Ru_3(\mu\text{-Cl})_3(CO)_9]^+$ models

The choice of $[Ru_3(\mu\text{-PH}_2)_3(CO)_9]^+$ of D_{3h} symmetry [see Scheme 1(*a*)] as the first computed model comes from the fact that most of the known 50-MVE triangular clusters have bridging phosphido ligands (see Table 1*a*,*b*). This model is in fact strongly related to compound **5**.[6] The EHT-computed

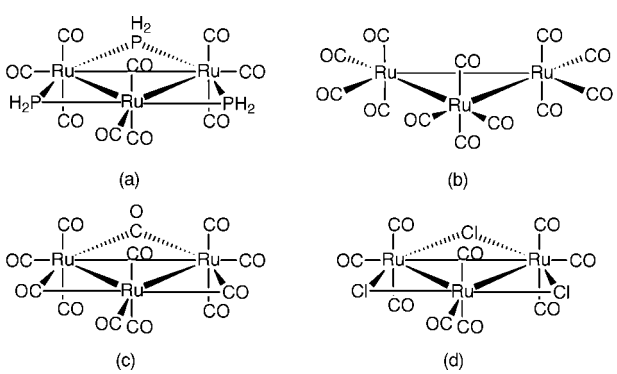

Scheme 1

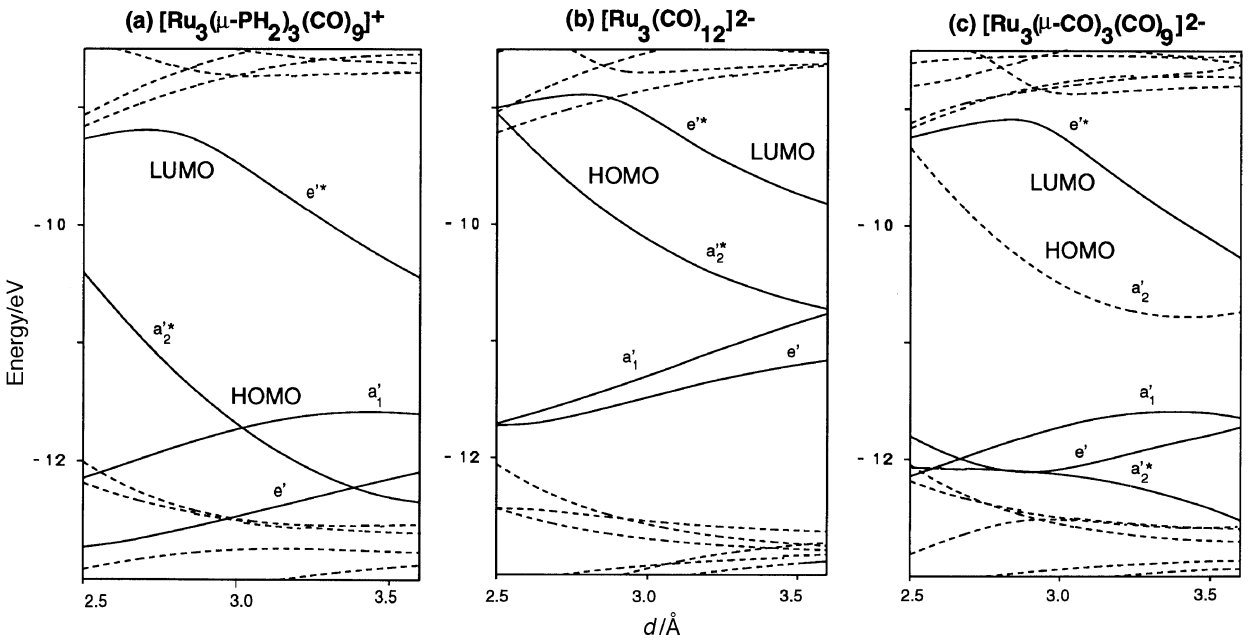

Fig. 2 EHT-computed Walsh diagram associated with the elongation of the Ru—Ru bonds (all the other geometrical parameters being kept constant) of the 50-MVE D_{3h} models: (*a*) $[Ru_3(\mu\text{-}PH_2)_3(CO)_9]^+$; (*b*) $[Ru_3(CO)_{12}]^{2-}$ (unbridged); (*c*) $[Ru_3(\mu\text{-}CO)_3(CO)_9]^{2-}$. Solid lines correspond to skeletal MOs.

Walsh diagram associated with the variation of the Ru—Ru distances from 2.5 Å to 3.6 Å, the M—P distances being kept constant, is shown in Fig. 2(*a*). The levels associated with the Ru—Ru bonds [see Fig. 1(*b*)] are represented by solid lines. Although the e′* and a_2'* levels exhibit parallel stabilization upon cluster expansion, e′* always stays high-lying while a_2'* remains at low energy. Regardless of the Ru—Ru separation, the HOMO–LUMO gap of this 50-MVE species is large. Since the EHT-optimized Ru—Ru distance (3.35 Å) was somewhat larger than the reported experimental values, calculations were carried out assuming Ru—Ru = 3.10 Å. The corresponding MO diagram is shown in Fig. 3(*b*). For this distance, the HOMO–LUMO gap is 2.03 eV. The total Ru—Ru overlap population is 0.062, a value indicative of a significant but still weak bonding. The Ru—Ru overlap population in each of the e′* LUMOs is −0.055. The corresponding value for the a_2'* level is −0.033. The in-phase occupied orbitals assumed to be responsible for the Ru—Ru bonding, namely e′ and a_1', have respective overlap values of 0.008 and 0.071. Clearly, the Ru—Ru bonding interaction is essentially contained in the a_1' HOMO.

It is interesting to note that, at the considered Ru—Ru distance, the significantly antibonding a_2'* orbital is situated below the bonding a_1' level. The a_2'* MO has a large metal participation (85%) of which more than 84% is from 4d AO. A rather similar situation is found for the in-phase e′ orbitals. This is not the case for the a_1' and e′* levels for which the 5p and 5s AOs contribute roughly one-third (e′*) or one-half (a_1') of the total metallic participation. This suggests that the energies of the 6 skeletal orbitals depend not only on their Ru—Ru bonding or antibonding nature, but also on their 5s/5p *vs.* 4d composition. This can be shown by a calculation in which all the Ru—Ru overlap integrals are set equal to zero. Such an artifact cancels all the Ru—Ru bonding and antibonding interactions. As a result, the bonding combinations are somewhat destabilized and the antibonding ones are stabilized, but some of these orbitals still remain far from each other. While the e′ and a_2'* orbitals become quasi-degenerate at ≈12.3 eV, the e′* LUMOs maintain a rather high energy (−10.18 eV), lying 1.14 eV above the a_1' HOMO.

The skeletal MO level ordering in $[Ru_3(\mu\text{-}PH_2)_3(CO)_9]^+$ can be conceptually reconstructed from the interaction of the frontier orbitals of the three metal centers lying in their local ligand environment. In the three $Ru(\mu\text{-}1/2PH_2)_2(CO)_3$ interacting fragments, the metal centers are in a local environment that is intermediate between capped square pyramidal and triangular bipyramidal (P—Ru—P = 158°). The frontier orbitals of such fragments are well-known.[27,28] They consist of a high-lying σ-type d/s/p hybrid and a set of three poorly hybridized d-type levels of π, π_σ and δ local symmetry, respectively. A good approximation for obtaining the frontier orbital diagram of the virtual $Ru(\mu\text{-}1/2PH_2)_2(CO)_3$ fragment is to extract a $Ru(PH_2)_2(CO)_3$ unit out of $[Ru_3(\mu\text{-}PH_2)_3(CO)_9]^+$ and to replace the two missing (μ-P)—Ru bonds on the phosphorus atoms by P—H bonds, without changing any bond angle.[29] The frontier orbital diagram of such a $Ru(PH_3)_2(CO)_3$ fragment, obtained by EHT calculations, is shown in Fig. 3(*a*). It is important to note that, due to its hybrid nature, the s-type frontier level lies largely above (1.88 eV) the d-type set. When the three $Ru(\mu\text{-}1/2PH_2)_2(CO)_3$ are brought together, the major interactions associated with Ru—Ru bonding are

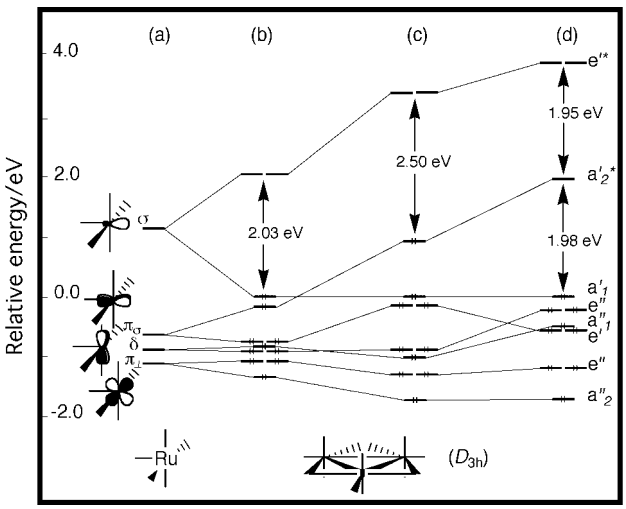

Fig. 3 Generation of the EHT-MO diagram of $[Ru_3(\mu\text{-}PH_2)_3(CO)_9]^+$ (*a*) from the interaction of the frontier orbitals of three $Ru(\mu\text{-}1/2PH_2)_2(CO)_3$ fragments and (*b*) assuming Ru—Ru = 3.1 Å. DFT level ordering of (*c*) $[Ru_3(\mu\text{-}PH_2)_3(CO)_9]^+$ and (*d*) $[Ru_3(\mu\text{-}PH_2)_3(CO)_9]^{3+}$. D_{3h} symmetry is considered.

afforded by the σ and π_σ frontier orbitals. By symmetry, a_1' is pure σ and a_2'* is pure π_σ. The bonding e′ orbitals are mainly π_σ in character with some σ admixture while the antibonding e′* orbitals have a dominant σ participation with some π_σ participation, mixed in a destabilizing way. The π and δ fragment orbitals yield more-or-less nonbonding combinations. It is clear from overlap considerations that the combinations of the σ hybrids are expected to exhibit a splitting larger than the combinations of the d-type π_σ orbitals. Therefore, e′* is expected to lie at high energy, always above the σ hybrid of the Ru(μ-1/2PH_2)$_2$(CO)$_3$ fragment from which it originates, even at large Ru—Ru separations. On the other hand, the d-type π_σ fragment orbitals being low-lying and contracted, their out-of-phase combination a_2'* is expected to remain at much lower energy. The resulting interaction diagram is shown in Fig. 3(*a*, *b*) still assuming Ru—Ru = 3.1 Å. Thus, it appears that the existence of a large HOMO–LUMO gap for the 50-MVE count requires two conditions: (*i*) non-negligible (although weak) overlap between the σ hybrids so that their in-phase a_1' combination stays at sufficiently low energy and (*ii*) π_σ orbitals on the metal centers that are essentially of d-type character (*i.e.*, low-lying and contracted).

Fig. 2(*a*) shows significant destabilization of the a_2'* orbital at short Ru—Ru separation, suggesting stability for the closed-shell 48-electron configuration [such as in Fig. 1(*a*)]. The EHT-optimized distance in $[Ru_3(\mu\text{-}PH_2)_3(CO)_9]^{2+}$ for this configuration is 2.84 Å. At this distance, the π_σ interaction is stronger and the Ru—Ru overlap population (0.132) is indicative of a real single bond. As a matter of fact, the related 48-MVE compound $Re_3(\mu\text{-}PPh_2)_3(CO)_9$ has been isolated and characterized (Re—Re = 2.91 Å).[30]

In order to bring a more quantitative overview to our EHT analysis, we have also carried out DFT calculations on the D_{3h} models $[Ru_3(\mu\text{-}PH_2)_3(CO)_9]^+$ and $[Ru_3(\mu\text{-}PH_2)_3(CO)_9]^{3+}$ (see Computational details). The major structural and electronic results corresponding to the optimized geometries are given in Table 2 and Fig. 2. It is clear from comparing Fig. 3(*b*) and 3(*c*) that both types of calculations are in a very good agreement. The optimized Ru—Ru separation of the 50-MVE cation is slightly longer than the corresponding average value of the related compound **5**.[6] DFT calculations found the a_2'* level to be the HOMO of the monocation with a large HOMO–LUMO gap (2.50 eV), in full agreement with EHT and experiment. The stability of the D_{3h} arrangement with respect to the open triangle was evaluated by doing several optimizations of $[Ru_3(\mu\text{-}PH_2)_3(CO)_9]^+$ in the C_{2v} and C_s symmetries. No significant distortion away from the regular triangular structure was found. However, the exploration of the potential energy surfaces indicates that small distortions away from the ideal D_{3h} symmetry require little energy.

DFT calculations found also a large HOMO–LUMO gap for the 48-MVE D_{3h} cation, suggesting stability for such species, but with significantly shorter M—M bonds. The metrical data optimized for $[Ru_3(\mu\text{-}PH_2)_3(CO)_9]^{2+}$ (Table 2) are consistent with the X-ray structure of the isoelectronic complex $Re_3(\mu\text{-}PPh_2)_3(CO)_9$.[30]

We have also investigated the electronic structure of the isoelectronic $[Ru_3(\mu\text{-}Cl)_3(CO)_9]^+$ D_{3h} model [Scheme 1(*b*)]. The EHT results (including the Walsh and MO diagrams) are very similar to those obtained for the isoelectronic $[Ru_3(\mu\text{-}PH_2)_3(CO)_9]^+$ model. At Ru—Ru = 3.1 Å, the corresponding overlap population is 0.067, with a HOMO-LUMO gap of 1.77 eV. Obviously, the triangular architecture appears to be able to house 50 MVEs. DFT calculations (Table 2) show also strong similarities between the phosphido- and chloro-bridged D_{3h} models. The DFT HOMO-LUMO gap is large (2.53 eV) and unique in the frontier MO region. The stability of the regular triangle with respect to the open triangle was evaluated by doing several optimizations in the C_{2v} and C_s symmetries. As for the phosphido relative, although the associated potential energy surface was found to be rather flat, no significant stabilization upon distortion away from the ideal D_{3h} symmetry was computed.

The unbridged 48-MVE and 50-MVE $[Ru_3(CO)_{12}]^{0/2-}$ models

48-MVE M_3L_{12} (M = Ru, Os) compounds are known to adopt the unbridged molecular structure exemplified by $Ru_3(CO)_{12}$ in Scheme 1(*c*).[1a–c,31] In order to understand why no unbridged 50-MVE cluster is known so far, we have investigated the electronic structure of the unbridged $[Ru_3(CO)_{12}]^{0/2-}$ systems. The EHT-computed Walsh diagram associated with the variation of the Ru—Ru distances is shown in Fig. 2(*b*). As for $[Ru_3(\mu\text{-}PH_2)_3(CO)_9]^+$, the e′* and a_2'* levels exhibit parallel stabilization upon cluster expansion. However, in contrast to the phosphido and chloro derivatives, the energy separation between these two levels is smaller and the a_2'* orbital never reaches a low energy. At a Ru—Ru separation of 3.1 Å, the a_2'* level lies 0.93 eV above the a_1' level and 1.04 eV below the e′* level. Even at this rather long distance, the 50-MVE count does not appear to be strongly favored. The EHT-optimized Ru—Ru distances are 2.68 and 2.93 Å for the 48-MVE and 50-MVE counts, respectively.

The high energy of the a_2'* orbital in $Ru_3(CO)_{12}$ can be easily understood by looking at its EHT MO diagram based on the interaction of three $Ru(CO)_4$ fragments, as shown in Fig. 4(*a*, *b*) for a Ru—Ru separation of 3.1 Å. It is well-known that an octahedron-derived ML_4 fragment has two frontier orbitals of σ and π_σ local symmetry, which are high-lying hybrids.[28,29] Therefore, even at very large Ru—Ru distances the a_2'* MO cannot be stabilized below the energy of the π_σ hybrids from which it derives. It follows that the unbridged M_3L_{12} architecture is not suitable for the 50-MVE count.

DFT geometry optimizations fully confirm the EHT analysis (see Table 2 and Fig. 4). A large HOMO-LUMO gap is computed for the 48-MVE $Ru_3(CO)_{12}$ cluster (2.84 eV) for which the computed Ru—Ru distances are close to the experimental ones.[31d,e] On the other hand, no large stabilization upon occupation of the a_2'* level is observed in the 50-MVE dianion of D_{3h} symmetry. Moreover, this regular triangular structure is unstable with respect to a bridged arrangement in which only two Ru—Ru bonds are present (see below).

Table 2 Major DFT-optimized bond distances (in Å) of the computed D_{3h} models $[Ru_3(\mu\text{-}X)_3(CO)_9]^{+/3+}$ (X = PH_2, Cl) and $[Ru_3(CO)_{12}]^{0/2-}$

Compound	MVE count	Ru—Ru	Ru—(μ-X)	Ru—$(CO)_{in\text{-}plane}$	Ru—$(CO)_{out\text{-}of\text{-}plane}$	C—$O_{bridging}$	C—$O_{in\text{-}plane}$	C—$O_{out\text{-}of\text{-}plane}$
$[Ru_3(\mu\text{-}PH_2)_3(CO)_9]^+$	50	3.169	2.379	1.906	1.957	—	1.142	1.140
$[Ru_3(\mu\text{-}PH_2)_3(CO)_9]^{3+}$	48	2.807	2.403	1.997	1.983	—	1.127	1.132
$[Ru_3(\mu\text{-}Cl)_3(CO)_9]^+$	50	3.012	2.405	1.920	1.971	—	1.138	1.136
$[Ru_3(\mu\text{-}Cl)_3(CO)_9]^{3+}$	48	2.710	2.397	2.082	2.009	—	1.121	1.127
$[Ru_3(CO)_{12}]^{2-}$ (unbridged)	50	3.272	—	1.917	1.942	—	1.167	1.158
$[Ru_3(CO)_{12}]$ (unbridged)	48	2.833	—	1.935	1.956	—	1.145	1.146
$[Ru_3(\mu\text{-}CO)_3(CO)_9]^{2-}$	50	3.102	2.154	1.879	1.941	1.187	1.167	1.159
$[Ru_3(\mu\text{-}CO)_3(CO)_9]$	48	2.922	2.144	1.913	1.968	1.159	1.149	1.142

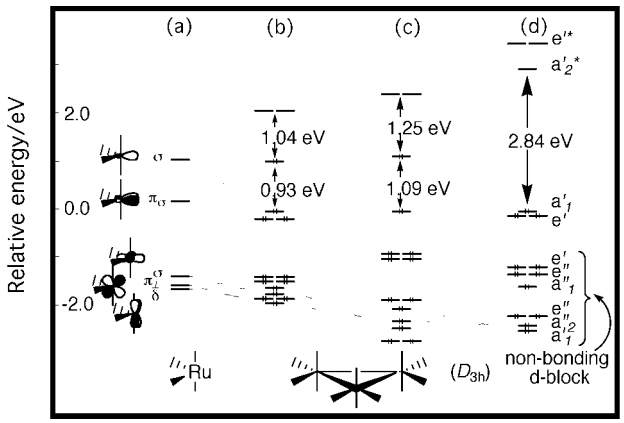

Fig. 4 Generation of the EHT-MO diagram of the unbridged cluster $Ru_3(CO)_{12}$ (*a*) from the interaction of the frontier orbitals of three $Ru_3(CO)_4$ fragments and (*b*) assuming Ru—Ru = 3.1 Å. DFT level ordering of (*c*) $Ru_3(CO)_{12}$ and (*d*) $[Ru_3(CO)_{12}]^{2-}$. D_{3h} symmetry is considered.

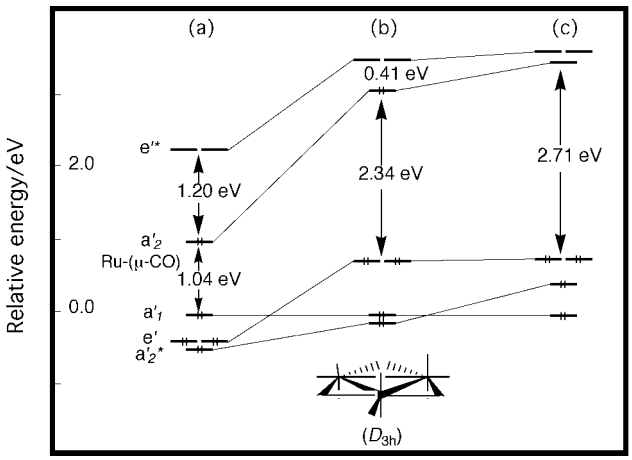

Fig. 5 EHT-MO diagram of the bridged cluster $Ru_3(\mu\text{-}CO)_3(CO)_9$ (*a*) assuming Ru—Ru = 3.1 Å. DFT level ordering of (*b*) $Ru_3(\mu\text{-}CO)_3(CO)_9$ and (*c*) $[Ru_3(\mu\text{-}CO)_3(CO)_9]^{2-}$. D_{3h} symmetry is considered.

The bridged 48-MVE and 50-MVE $[Ru_3(\mu\text{-}CO)_3(CO)_9]^{0/2-}$ models

Since bridging ligands appear to favor the 50-MVE count, we have investigated the stability of a bridged 50-MVE $[Ru_3(CO)_{12}]^{2-}$ species. The EHT-computed Walsh diagram associated with the variation of the Ru—Ru distances of this arrangment is shown in Fig. 2(*c*). At first sight, it looks quite similar to the one of the unbridged $Ru_3(CO)_{12}$ system [Fig. 2(*b*)], with an a'_2 level stabilized upon cluster expansion, but still remaining at high energy. It turns out, however, that this a'_2 level is not a skeletal MO, but one of the 6 bonding Ru—(μ-CO) orbitals that are expected to be occupied, even in the 48-MVE species [there are 6 Ru—(μ-CO) bonds]. The other 5 Ru—(μ-CO) MOs lie at lower energy. This high-lying a'_2 orbital is mainly derived from a π*(CO) combination, stabilized by a 5p(Ru) combination. Because of the high energy of the π*(CO) orbitals and poor overlap with the metal 5p AOs, this Ru—(μ-CO) bonding combination remains at high energy and is not occupied for the 48-MVE count when considering large Ru—Ru separations. Rather, it is the low-lying skeletal a'_2* MO that is occupied. Indeed, the level ordering of the skeletal MOs in $[Ru_3(\mu\text{-}CO)_3(CO)_9]^{0/2-}$ is very similar to that of $[Ru_3(\mu\text{-}PH_2)_3(CO)_9]^{+/3+}$ [Fig. 3(*a*, *b*)]. In other words, when going from the phosphido-bridged to the carbonyl-bridged cluster, there is a level crossing between two a'_2 orbitals of very different nature, at least at large Ru—Ru separation.[32] They mix somewhat at short Ru—Ru distances, starting progressively to exchange their character below Ru—Ru ≈ 2.8 Å and consequently providing a significant HOMO–LUMO gap for the 48-MVE count. This D_{3h} bridged structural arrangement is, however, unlikely to favor the 50-MVE count since the a'_2 Ru—(μ-CO) bonding level remains high in energy, even at very large Ru—Ru separations.

DFT geometry optimizations are in good agreement with the EHT calculations (see Table 2 and Fig. 5). A large HOMO–LUMO gap is computed for the 48-MVE $Ru_3(\mu\text{-}CO)_3(CO)_9$ cluster (2.71 eV). On the other hand, adding two electrons does not significantly stabilize the a'_2 HOMO in the optimized 50-MVE D_{3h} species. Consistent with the nature of this HOMO, the optimized Ru—Ru separations of the 48-MVE and 50-MVE species are not very different (Table 2). Moreover, frequency calculations performed on these D_{3h} geometries indicated that $Ru_3(\mu\text{-}CO)_3(CO)_9$ is a true minimum, while the dianion yielded an imaginary frequency. When the symmetry constraint of the triply bridged dianion is lowered to C_{2v} or C_s, the geometry optimization leads to a structure in which one Ru—Ru bond is broken. The lowest energy was found for a geometry close to C_{2v} but of exact C_s symmetry presenting two short intermetallic separations of 2.930 Å and one long nonbonding contact of 3.79 Å. This open structure is more stable than the D_{3h} arrangement by 0.51 eV. An even lower energy was found for an open triangular structure in which there are only two μ-CO ligands bridging the same Ru—Ru edge. In this C_1 arrangement, which can be derived from the one of $Fe_3(CO)_{12}$[33] by breaking one metal–metal bond, the Ru—Ru separations are equal to 2.97 (bridged), 3.10 and 4.38 Å. It is more stable than the D_{3h} form by 1.02 eV. Because of the bridging *vs.* terminal versatility of the carbonyl ligands in these species,[33b] it was not possible to fully explore the potential energy surface of $[Ru_3(CO)_{12}]^{2-}$. Nevertheless, these results show clearly that simply the presence of carbonyl (or other π-acceptor) ligands favors the open triangular electron-precise form.

Electronic characteristics of the known 50-MVE M_3L_n triangular clusters and related compounds

In order to check the consistency of the results described above over the whole series of reported 50-MVE triangular complexes, we have carried out EHT calculations on all the experimental crystal structures that were available electronically through the Cambridge Data Base system[23] (see Computational details) for this type of compound. Clusters of higher nuclearity but containing a 50-MVE triangle for which the other metal centers can be considered as part of its ligand system were also included in our analysis. The major results are given in Table 1(*a*,*b*). In all the computed compounds the HOMO–LUMO gap is the unique large-energy gap in the frontier orbital region. In most of them the HOMO resembles the a'_1 HOMO of $[Ru_3(\mu\text{-}PH_2)_3(CO)_9]^+$ while the second or third HOMO resembles the a'_2*. The M—M overlap populations of the 50-MVE M_3 systems [Table 1(*a*)] are all in the range of weak bonding, as for the $[Ru_3(\mu\text{-}PH_2)_3(CO)_9]^+$ model. There is no significant bonding in **5**, as well as for one Rh—Rh bond in **8** for which the two other bonds are very weak. Clearly, the relative strength of the weak M—M interaction is tuned by the nature of the ligands (compare the closely related compounds **7** and **8**, for example). It appears also that weak bonding (or even no bonding at all) within the M_3 triangle does not affect the width of the HOMO–LUMO gap, which always remains large. For example, in the case of **5** there are two nearly degenerate LUMOs that can be very clearly identified as being e'*, while the fourth HOMO corresponds to a'_2*. Although these orbitals are all weakly antibonding in **5**, they are separated by an energy gap of 2.21 eV

because of their different nature (σ-hybrid *vs.* pure d-type). One is in the situation of $[Ru_3(\mu\text{-}PH_2)_3(CO)_9]^+$ at very large Ru—Ru separation (left side of Fig. 2).

The metal-bridged 50-MVE triangular systems [Table 1(*b*)] present similar characteristics. The M—M bonding is somewhat stronger, especially in the case of the metal-bridged bond. This peculiarity has been analyzed by others[11b,12] and is due to a donation from the $a_2'^*$ orbital (and some other MOs) into an empty frontier orbital of the bridging organometallic ligand. Bridging a 50-MVE triangle by a d^8 ML_4 unit helps to release its electron richness.

Platinum and palladium M_3L_n clusters usually exhibit planar coordination with 16-electron metal centers. For these species, the MVE count associated with 3 localized M—M single bonds is 42. This number corresponds to the electron-precise 48-MVE count after having depopulated 3 non-bonding metal orbitals, the skeletal electronic structures being related in both systems. Adding 2 extra electrons to planar 42-MVE clusters renders them analogous to the title 50-MVE compounds, with respect to M—M bonding. Previous theoretical studies have shown that the a_2' MO is indeed occupied in these 44-MVE systems.[16,17,34,35] These compounds are listed in Table 1(*c*,*d*) together with their reported M—M bond distances and some EHT-computed data. Note that other 44-MVE M_3L_n clusters, which are not electron-rich with respect to M—M bonding, are not considered in this study.[1i–k,36] For example, there are 44-MVE electron-precise triangular systems made of the assembly of one 18-electron and two planar 16-electron centers.[36] Compound **19**[15] could also have a different electronic structure, but the lack of available structural data prevented us from calculating it.

The data of Table 1(*c*,*d*) are quite similar to those of Table 1(*a*,*b*). The computed Pt—Pt overlap populations are larger than any other M—M values (Table 1). This may be partly due to an artifact of the method or of the choice of atomic parameters. Nevertheless, one can see that compound **22**, which has its 3 Pd—Pd bonds bridged by $Fe(CO)_4$ units, exhibits larger Pt—Pt overlap populations than for the other Pt_3 systems. This is the consequence of a large electron transfer from $a_2'^*$ into the $Fe(CO)_4$ accepting orbitals. In this compound there is extensive delocalization of the extra electrons over the whole Pt_3Fe_3 framework.

Finally, it is noteworthy that in all the listed compounds (except **1** and **2**) there are approximately in-plane bridging ligands, associated with large bridge—M—bridge angles, that provide the metal center with a low-lying π_σ d-type frontier orbital and a high-lying σ hybrid. The closely related compounds **1** and **2** are different from the other clusters in that the metal centers lie in a local distorted octahedral environment with both σ and π_σ being members of the t_{2g} set.[3] It turns out that the distortion of the local octahedral ligand sphere splits the t_{2g} degeneracy in such a way that σ lies ≈0.5–0.6 eV above π_σ. Moreover, the orientation of the local octahedra with respect to the M_3 triangle is such that the two sides of the Mo_3 triangle are inequivalent. This renders the π_σ frontier orbitals partly out-of-plane and their ovelap partly δ-type in character. On the other hand, plots of the σ frontier orbitals indicate that they remain approximately in-plane, presumably due to the distortion of the local octahedra. These factors are sufficient for creating a significant splitting between e′* and $a_2'^*$ and consequently a large HOMO–LUMO gap for 50-MVEs. Clearly, the 50-MVE clusters **1** and **2** have enough geometrical flexibility to allow them to adjust their molecular structure to fullfill the closed-shell requirement.

Conclusions

The studied 50-MVE triangular clusters exhibit weak or very weak M—M bonding, mainly contained in the a_1' MO. Nevertheless, the HOMO–LUMO gap always remains large. This is due to the fact that, at the considered internuclear separations, the weakly antibonding $a_2'^*$ level remains at low energy [Fig. 1(*b*)] due to its d-type nature. On the contrary, the out-of-phase e′* orbitals are maintained at high energy, mainly because of their s/p/d hybrid nature, while their in-phase a_1' counterparts maintain sufficiently bonding character to stay low-lying. The hybrid *vs.* pure d character of the frontier orbitals on the metal centers is controlled by the geometry of the ligand environment (in particular, the presence of in-plane μ_2-ligands with large bridge—M—bridge angles). However, bridging π-acceptor ligands do not appear to favor 50-MVE counts, at least for M = Ru and probably for other group VIII metals. This may be the reason why the 50-MVE cluster $Ru_3(\mu_3\text{-}\eta^2\text{-}PPhpy)(\mu\text{-}PPh_2)(CO)_9$, closely related to compound **3** but having only one phosphido bridge, adopts the open triangular electron-precise structure.[37] The presence of the bridges also helps to maintain the weakly bound metal centers together, although they cannot always prevent the M_3 triangle from opening. A nice example of cluster core isomerism has been shown to exist and investigated theoretically in the case of compound **20**.[16] Our EHT calculations on the open form of **20** lead to Pt—Pt overlap populations (0.162) that are much larger than in the closed form (averaged value = 0.084). The value corresponding to the open Pt···Pt edge indicates no bond (0.000). A similar result is found for the open triangular $Ru_3(\mu_3\text{-}\eta^2\text{-}PPhpy)(\mu\text{-}PPh_2)(CO)_9$ cluster[37] (corresponding values 0.156, 0.177 and −0.017), as compared to the related triangular cluster **3** (averaged value = 0.049).

Acknowledgements

We thank Dr J.-F. Halet for helpful comments. Computing facilities were kindly provided by the IDRIS-CNRS computing center of Orsay (France). The CNRS (J.-Y. S.) and CONICYT (M. T. G.) are acknowledged for a cooperative French/Chilean travel grant.

Notes and references

1 See for example (and references therein): (*a*) *Transition Metal Clusters*, ed. B. F. G. Johnson, J. Wiley, New York, 1980; (*b*) *Metal Clusters*, ed. M. Moskovits, J. Wiley, New York, 1986; (*c*) F. A. Cotton and R. A. Walton, *Multiple Bonds Between Metal Atoms*, Clarendon Press, Oxford, 1993; (*d*) B. E. Bursten, F. A. Cotton, J. C. Green, E. A. Seddon and G. G. Stanley, *J. Am. Chem. Soc.*, 1980, **102**, 955; (*e*) B. E. Bursten, F. A. Cotton, M. B. Hall and R. C. Najjar, *Inorg. Chem.*, 1982, **21**, 302; (*f*) F. A. Cotton and X. Feng, *Inorg. Chem.*, 1991, **30**, 3666; (*g*) Y. Jiang, A. Tang, R. Hoffmann, J. Huang and J. Lu, *Organometallics*, 1985, **4**, 27; (*h*) C. Mealli, *J. Am. Chem. Soc.*, 1985, **107**, 2245; (*i*) M. A. Arif, J. G. Hefner, R. A. Jones, T. A. Albright and S. A. Kang, *J. Am. Chem. Soc.*, 1986, **108**, 1701; (*j*) K. Tsuge, S. Yajima, H. Imoto and T. Saito, *J. Am. Chem. Soc.*, 1992, **114**, 7910; (*k*) G. Süss-Fink, I. Godefroy, V. Ferrand, A. Neels, H. Stoeckli-Evans, S. Kahlal, J.-Y. Saillard and M. T. Garland, *J. Organomet. Chem.*, 1999 in press.
2 M. Shieh, F.-D. Mia, S.-M. Peng and G. H. Lee, *Inorg. Chem.*, 1995, **34**, 5455.
3 J. W. van Hal, K. H. Whitmire, B. Zouchoune, J.-F. Halet and J.-Y Saillard, *Inorg. Chem.*, 1995, **34**, 5455.
4 N. Lugan, P.-L. Fabre, D. de Montauzon, G. Lavigne, J.-J. Bonnet, J.-Y Saillard and J.-F. Halet, *Inorg. Chem.*, 1993, **32**, 1363.
5 J. A. Cabeza, F. J. Lahoz and A. Martin, *Organometallics* , 1992, **11**, 2754.
6 J. F. Corrigan, S. Doherty, N. J. Taylor, A. J. Carty, E. Boroni and A. Tiripicchio, *J. Organomet. Chem.*, 1993, **462**, C24.
7 A. A. Cherkas, N. J. Taylor and A. J. Carty, *J. Chem. Soc., Chem. Commun.*, 1990, 385.
8 R. J. Haine and N. C. D. T. Streen, *J. Chem. Soc., Dalton Trans.*, 1984, 515.
9 A. J. Carty and S. A. MacLaughin, *Organometallics* , 1982, **1**, 1013.
10 M. R. Churchill, C. Beuno and D. A. Young, *J. Organomet. Chem.*, 1981, **213**, 139.
11 (*a*) J. F. Corrigan, M. Dinardo, S. Doherty, G. Hogarth, Y. Sun, N. J. Taylor and A. J. Carty, *Organometallics*, 1994, **13**, 3572; (*b*) J. F. Corrigan, Y. Sun and A. J. Carty, *New. J. Chem.*, 1994, **18**, 77.

12 A. M. Arif, D. E. Heaton, R. A. Jones and C. M. Nunn, *Inorg. Chem.*, 1987, **26**, 4228.
13 D. E. Berry, G. W. Bushnell, K. R. Dixon, P. M. Moroney and C. Wan, *Inorg. Chem.*, 1985, **24**, 2625.
14 G. W. Bushnell, K. R. Dixon, P. M. Moroney, A. D. Rattray and C. Wan, *J. Chem. Soc., Chem. Commun.*, 1977, 709.
15 S. Otsuka, Y. Tatsuno and M. Miki, *J. Chem. Soc., Chem. Commun.*, 1973, 445.
16 R. Bender, P. Braunstein, A. Dedieu, P. Ellis, B. Huggins, P. D. Harvey, E. Sappa and A. Tiripicchio, *Inorg. Chem.*, 1996, **35**, 1223.
17 S. G. Bott, M. F. Hallam, O. J. Ezomo, D. M. P. Mingos and I. D. Williams, *J. Chem. Soc., Dalton Trans.*, 1988, 1461.
18 G. Longoni, M. Manassero and M. Sansoni, *J. Am. Chem. Soc.*, 1980, **102**, 7973.
19 C. Mealli and D. Proserpio, *J. Am. Chem. Soc.*, 1990, **112**, 5484.
20 R. Hoffmann, *J. Chem. Phys.*, 1963, **39**, 1397.
21 C. Mealli and D. Proserpio, *J. Chem. Educ.*, 1990, **67**, 399.
22 J. H. Ammeter, H.-B. Bürgi, J. C. Thibeault and R. Hoffmann, *J. Am. Chem. Soc.*, 1978, **100**, 3686.
23 Cambridge Data Base System, Cambridge Crystallographic Data Center, Version 5.12.
24 (*a*) E. J. Baerends, D. E. Ellis and P. Ros, *Chem. Phys.*, 1975, **8**, 41; (*b*) E. J. Baerends and P. Ros, *Int. J. Quantum Chem.*, 1978, **S12**, 169; (*c*) P. M. Boerrigter, G. te Velde and E. J. Baerends, *Int. J. Quantum Chem.*, 1988, **33**, 87; (*d*) G. te Velde and E. J. Baerends, *J. Comput. Phys.*, 1992, **99**, 84.
25 *Amsterdam Density Functional (ADF) Program*, version 2.3, Vrije Universiteit, Amsterdam, Netherlands, 1997.
26 S. D. Vosko, L. Wilk and M. Nusair, *Can. J. Chem.*, 1990, **58**, 1200.
27 R. Hoffmann, *Angew. Chem., Int. Ed. Engl.*, 1982, **21**, 711.
28 T. A. Albright, J. K. Burdett and M.-H. Whangbo, *Orbital Interactions in Chemistry*, John Wiley and Sons, New York, 1985.
29 In a previous study[4] we considered the $Ru(PH_2)_2(CO)_3$ fragment as a model for the $Ru(1/2PH_2)_2(CO)_3$ building block. It turns out that this leads to an underestimation of the metal participation in π_σ. In the $Ru(PH_3)_2(CO)_3$ model, this participation is very large (97%).
30 H.-J. Haupt, P. Balsaa and U. Flörke, *Inorg. Chem.*, 1988, **27**, 280.
31 (*a*) R. Mason and A. I. M. Rae, *J. Chem. Soc. A.*, 1968, 778; (*b*) R. E. Corey and L. F. Dahl, *Inorg. Chem.*, 1962, **1**, 521; (*c*) M. R. Churchill and B. G. DeBoer, *Inorg. Chem.*, 1977, **16**, 878; (*d*) M. R. Churchill, F. J. Hollander and J. P. Hutchinson, *Inorg. Chem.*, 1977, **16**, 2655; (*e*) M. L. Bruce, M. J. Liddell, O. bin Shawkataly, C. A. Hughes, B. W. Skelton and A. L. White, *J. Organomet. Chem.*, 1988, **347**, 207.
32 This point was not clearly established in our previous study of this model.[4]
33 (*a*) F. A. Cotton and J. M. Troup, *J. Am. Chem. Soc.*, 1974, **96**, 4155; (*b*) D. Braga, F. Grepioni, L. J. Farrugia and B. F. G. Johnson, *J. Chem. Soc., Dalton Trans.*, 1994, 2911.
34 D. J. Underwood, R. Hoffmann, K. Tatsumi, A. Nakamura and Y. Yamamoto, *J. Am. Chem. Soc.*, 1985, **107**, 5968.
35 (*a*) D. I. Gilmour and D. M. P. Mingos, *J. Organomet. Chem.*, 1986, **302**, 127; (*b*) D. M. P. Mingos and T. Lee, *J. Organomet. Chem.*, 1990, **394**, 679.
36 (*a*) V. G. Albano and G. Ciani, *J. Organomet. Chem.*, 1974, **66**, 311; (*b*) A. Albinati, G. Carturan and A. Musco, *Inorg. Chim. Acta*, 1976, **16**, L3; (*c*) M. F. Hallam, N. D. Howells, D. M. P. Mingos and R. W. M. Wardle, *J. Chem. Soc., Dalton Trans.*, 1985, 845; (*d*) R. Ramachandran, D.-S. Yang, N. C. Payne and R. J. Pudephatt, *Inorg. Chem.*, 1992, **31**, 4236.
37 N. Lugan, G. Lavigne, J.-J. Bonnet, R. Réau, D. Neibecker and I. Tkatchenko, *J. Am. Chem. Soc.*, 1998, **110**, 5369.

Paper 9/00421A